Orbital-dependent spin textures in Bi_{2}Se_{3} quantum well states

Chiu-Yun Lin, Kenneth Gotlieb, Chris Jozwiak, Jonathan A. Sobota, Zhi-Xun Shen, James G. Analytis, Zahid Hussain, and Alessandra Lanzara

Phys. Rev. B **98**, 075149 — Published 27 August 2018

DOI: 10.1103/PhysRevB.98.075149

Orbital-dependent spin textures in Bi_2Se_3 quantum well states

Chiu-Yun Lin,[1,2,*] Kenneth Gotlieb,[3,2,†] Chris Jozwiak,[4,‡] Zahid Hussain,[4,§] and Alessandra Lanzara[1,2,¶]

[1] *Department of Physics, University of California, Berkeley, California 94720, USA*
[2] *Materials Sciences Division, Lawrence Berkeley National Laboratory, Berkeley, California 94720, USA*
[3] *Graduate Group in Applied Science & Technology, University of California, Berkeley, California 94720, USA*
[4] *Advanced Light Source, Lawrence Berkeley National Laboratory, Berkeley, California 94720, USA*

(Dated: July 31, 2018)

Understanding the fine interplay between spin and orbital degrees of freedom in the surface states of topological insulators is the key to the development of next generation spintronics devices. So far the majority of studies have focused on the helical spin texture of the topologically protected surface state (TSS) and little attention has been devoted to the spin texture of the other surface states: the bulk-originated quantum well states (QWSs). This work presents the first of such study in a prototypical topological insulator, Bi_2Se_3. By using spin and angle resolved photoemission spectroscopy we reveal a full momentum dependent spin texture of the QWSs and their response to light polarization. We find that these states share a similar spin-orbital texture with the TSS. This work shows an intimate correlation between the surface and bulk states, which was overseen before, and provides new relevant information to understand how the surface states evolve with the bulk states.

I. INTRODUCTION

The interplay between spin-orbit interaction (SOI) and structural symmetry has become one of the most active topics in condensed matter physics. Under this circumstance, topological insulators (TIs) have attracted extensive attention because of their exotic properties[1–3] as well as their potential in device applications and quantum computation[4–7]. The crystal symmetries and strong SOI, which mixes the orbital and spin degrees of freedom, not only provide levers to control spin[8] but also enable intriguing phenomena including quantum anomalous Hall effect[9,10], spin galvanic effect[11], and magneto-optical Kerr effect[12].

Nevertheless, the onset of some of these exciting effects requires incorporating TIs into a heterostructure device or conducting doping treatments on the crystal surfaces. Under these conditions, a potential gradient can develop at the TI surface[13,14]. This will trap the bulk-originated electrons by pushing bands to deeper binding energy near the surface. As a result, new states can emerge due to the quantization of the bulk conduction and valence bands[15,16], giving rise to the development of well defined quantum well states (QWSs). These states can be easily induced under a variety of conditions, such as surface exposure of ambient environment or surface absorption of various adatoms including gas molecules[14,15,17], alkali metals[16,18], and other donor species like Fe[13]. The resulting two-dimensional electron gases not only coexist with the topological surface state (TSS) electrons near the surface, their spin degeneracy can also be lifted by the Rashba effect[14–17].

Understanding the spin-orbital entanglement of these additional two dimensional carriers is critically essential for the design of spin-based device and understanding the interplay between the charge and spin transport. Spin- and angle-resolved photoemission spectroscopy (SARPES)[19,20] provides a unique opportunity to map the orbital-dependent spin textures of a material by measuring the spins of distinct orbital components that are selectively photoemitted with different light polarizations[21,22]. Specifically, one can unravel the intertwined spin and orbital degrees of freedom in a strong SOI system by exploiting light-dependent matrix elements in scattering processes[23,24] while measuring the spin polarization of the photoelectrons[8,25–28]. Since the spin is preserved in p- to s-wave transitions[21], this provides a hint to the entanglement of spin textures and orbitals in the initial state.

So far, a systematic mapping of spin-orbital characteristics of the complete surface states (including TSS and QWSs) after the quantization of the bulk bands is lacking. In the present work, we present the orbital-dependent spin textures of a prototypical three-dimensional TI, Bi_2Se_3, using SARPES. Our results provide a foundation for spin-based device applications of Bi_2Se_3 as well as insight about the role of SOI in a material at the atomic level.

II. METHODS

A clean Mg-doped p-type Bi_2Se_3 surface was created by cleavage in ultrahigh vacuum chamber under the baseline pressure of $\approx 5 \times 10^{-11}$ Torr at ≈80 K. The surface experienced a pressure burst, caused by an explosion of magnesium pocket irradiated with intense infrared pulse. Mg particles effectively doped the sample surface to n-type leading to quantization of the conduction band. A similar effect has been reported in earlier works[14,16].

Spin-and angle-resolved photoemission measurements (SARPES) are performed utilizing a high-efficiency spin-resolved photoelectron spectrometer[19,20] coupled to a lab-based 4^{th} harmonic 5.99eV laser generated from a

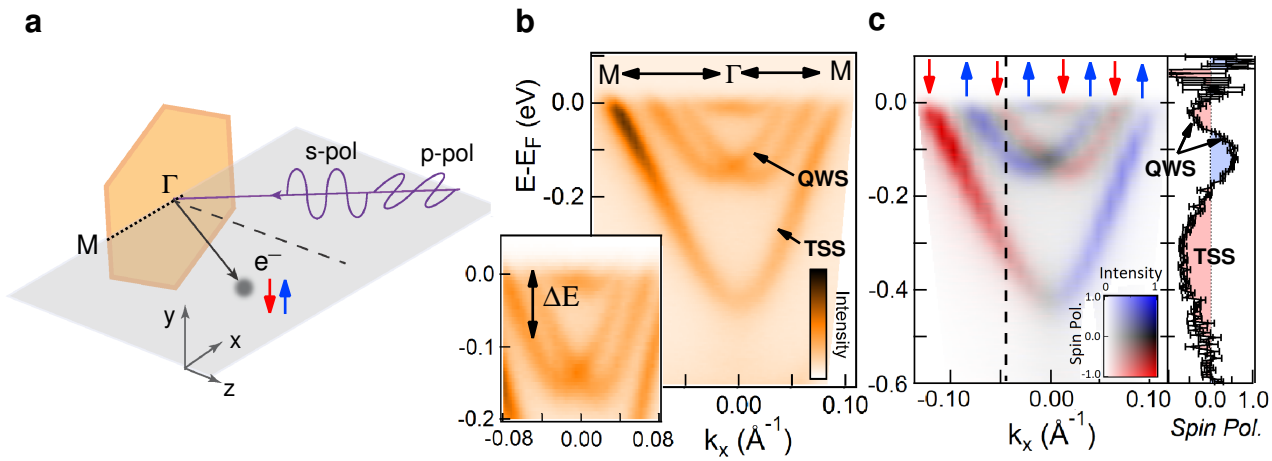

FIG. 1. Diagram of experimental geometry is shown in **(a)**. Blue and red arrows illustrate the measured in-plane spin-up/down components, P_y. Figure **(b)** shows an ordinary ARPES band dispersion map along $\bar{\Gamma}$-$\bar{M}$ by s-polarized photons, where TSS and QWSs can be clearly observed. A large Rashba splitting $\Delta E = 105$ meV at k_F can be observed in the zoomed in panel of **(b)**. The same map but collected with a spin-polarimeter is presented in **(c)**, in which the color represents spin polarization while brightness shows the intensity. The spin polarization dispersion at a selected momentum is attached to the spin-resolved map. One can examine the spin polarization for each surface bands.

cavity-dumped Ti:sapphire oscillator. This combination enables rapid high-resolution data acquisition with ≈ 16 meV energy resolution and ± 0.02 Å^{-1} momentum resolution.

The experimental geometry is illustrated in Fig. 1(a). S- (linear vertical, $\hat{e}$ along y axis) and p-polarized (linear horizontal, $\hat{e}$ in x-z plane) light is shone on the crystal. The energy and the in-plane, vertical spin component (S_y) of photoelectrons emitted along z axis are measured by the spectrometer. A band dispersion map is acquired by rotating the sample polar angle along the y axis with respect to the fixed spectrometer. The measured spin-up and spin-down components are depicted with blue and red arrows, respectively. The spin polarization is the normalized difference of spin-up and spin-down intensity, $P_y = (I_\uparrow - I_\downarrow)/(I_\uparrow + I_\downarrow)$.

III. RESULTS

The spin-integrated and spin-resolved maps of Bi_2Se_3 along $\bar{\Gamma}$-$\bar{M}$ are shown in Fig. 1(b)(c), respectively. In addition to the well known TSS, a pair of parabolic dispersive bands are resolved. The latter are QWSs that stem from the band bending effect due to the doping of extrinsic impurities that induces conduction band quantization. The presence of a large potential gradient across the doped surface and the strong intrinsic SOI in Bi_2Se_3 shift the two QWS branches away from $\bar{\Gamma}$-point yielding a large splitting $\Delta E = 105$ meV at $k_F = 0.05$ Å^{-1} as shown in the inset of Fig. 1(b).

The splitting can be explained within the Rashba SOI model of a two-dimensional electron gas, $E_\pm(k_{||}) = E_0 + \frac{\hbar^2 k_{||}^2}{2m^*} \pm \alpha_R k_{||}$, where m* is the effective mass and α_R is the Rashba parameter, a material-dependent phenomenological prefactor determined by the strength of SOI and potential gradient. The latter can be extracted experimentally from the Rashba term ($\alpha_R k_{||}$) by measuring the energy difference of a pair of split bands. Fig. 1(b) yields a large Rashba parameter $\alpha_R = 2.4$ eVÅ, which is one to two orders of magnitude larger than 2DEG in conventional semiconductors and 3–4 times larger than Au, $\alpha_R = 0.63$ eVÅ[8,20,29].

Fig. 1(c) presents a spin-resolved version of Fig. 1(b), where the color shows the spin polarization and the brightness represents intensity of photoelectrons. One can see that each TSS and QWS subbands possess opposite spins to its adjacent bands, and the polarization magnitude of each band along the selected momentum cut is shown in the plot of spin polarization dispersion attached to the map.

In figure 2, we show the photon polarization dependent spin characters of the QWSs for two distinct photon polarization geometries. For simplicity, the inner and outer subbands of the first QWS, and the TSS are denoted by α, β, γ symbols, respectively. Interestingly, the spin characters with opposite signs are observed in QWSs when the light polarization is rotated by $\pi/2$ just like the TSS band[8]. This can be easily observed from the spin-resolved intensity maps (panels (a)(b)) as well as the relative intensity of the spin-resolved energy dispersion curves (EDCs) in panels (c)(d) along selected momenta $k_x = \pm k_1$. Panels (e-h) show the corresponding measured spin polarization of the EDCs. In (e)(g), one can see the α branch (the first peak near E$_F$) shows $P_y =$ 55% with s-polarized photons but $P_y =$ -50% is measured with p-polarized photons, and vice versa for the β band.

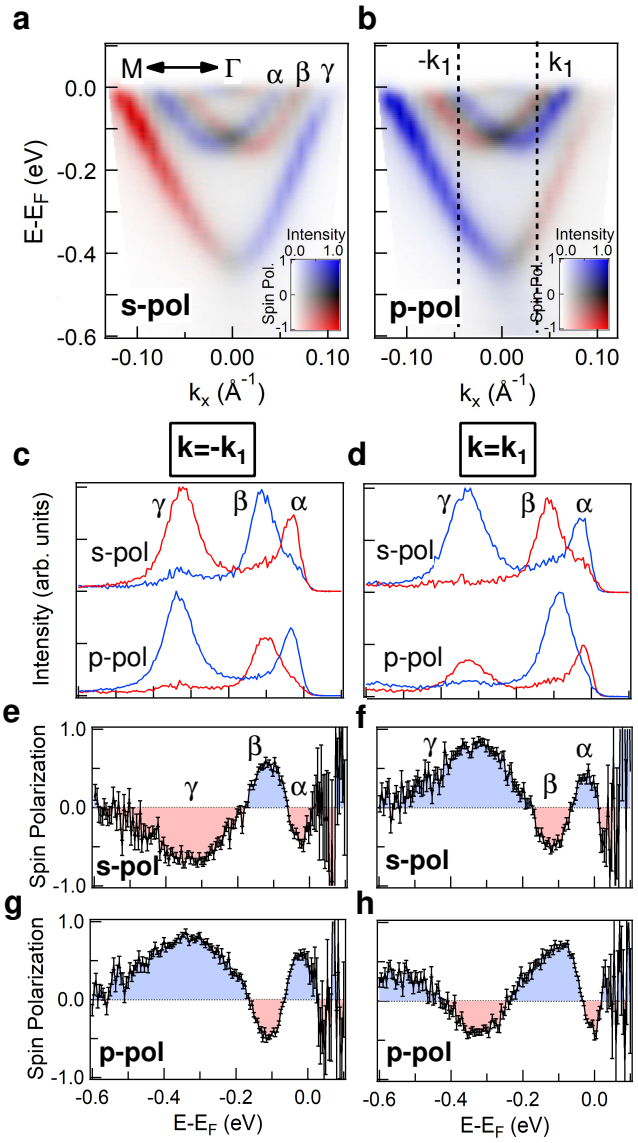

FIG. 2. Spin-resolved maps of Bi_2Se_3 surface states along $\bar{\Gamma}$-$\bar{M}$ made with s- and p-polarized light are presented in **(a)(b)**, respectively. S- and p-polarized photons reveals opposite spins of both the TSS and QWSs. The spin-resolved EDCs at momenta $k = \pm k_1$ are shown in **(c)** and **(d)**, and the correspondent spin polarizations are shown in **(e-h)**. The intensity and spin polarization of the inner, outer 1^{st} QWS, and TSS band, denoted with symbol α, β, γ, respectively, can be clearly observed.

A similar phenomenon can be observed on the other side of $\bar{\Gamma}$ as shown in Fig. 2(f)(h). Notice the offset to positive spin polarization in Fig. 2(g)(h). This is a consequence of spin-dependent photoemission dipole matrix elements effect due to the experimental geometry[30].

IV. DISCUSSIONS

The observed inverted spins in QWSs and the alternating spin helicities of TSS and QWSs can be simultaneously explained from the aspect of the time-reversal symmetry constraint in Bi_2Se_3 or by obital analysis at the atomic level.

From the former prospective, since spin degeneracy is required at high symmetry points, two split bands can only pair up with opposite spin helicity. As calculations have shown, TSS and QWS split bands will switch their pairing partner from $\bar{\Gamma}$ to $\bar{M}$[31]. Namely, the TSS and the outer branch of the 1^{st} QWS are degenerate at $\bar{M}$. Therefore, given the fact that the TSS shows opposite spins with respect to different photon polarization[8], the spin of QWSs has to change its sign correspondingly.

Alternatively, using the same theoretical framework for the TSS in Ref.[21,22], one can calculate the orbital-dependent spin textures, which describes the spin characters of a selected orbital for the bands in momentum space. The calculation of the orbital-dependent spin texture can be simplified by only considering the matrix elements of the Hamiltonian term that will affect the spin, $\hat{H}_{eff} \propto \vec{A} \cdot \vec{p} \propto \hat{e} \cdot (\vec{s} \times \nabla V)$, where $\vec{A}$ characterizes the incident radiation, $\vec{p}$ is the dipole moment, and ∇V represents the potential gradient. Since QWSs and TSS share the same effective Hamiltonian due to the identical symmetry contraints, and the same orbitals that are involved in the SARPES measurements, these suggest QWSs and TSS carry identical orbital-dependent spin textures. Specifically, the measured spin characters of TSS and QWSs will qualitatively show similar response to the rotation of photon polarization being governed by the same effective Hamiltonian in the Rashba-SOI form.

The same effective Hamiltonian and switching of the pairing band[31] imply an intimate connection between TSS and QWSs. This is in agreement with the spin observations on the unoccupied surface resonance states[32] and the Rashba-like nature of trivial gapped surface states in topological phase transitions studies[33,34]. It has been shown that the bulk-derived USR exhibits a strong surface-localized component that is closely related to the TSS as they evolve from a pair of Rashba-like states through the band inversion[32]. The essential difference between the connection of TSS to QWSs and USR is the QWS electrons are indeed constrained to the surface. This further explains the observed alternating spin helicies of TSS and QWSs, where one can take the spin of TSS as an analogy to the inner subband of a Rashba-like gapped states that is adjacent to another Rashba-split band (the outer subband of QWS). Still, the Rashba-like gapped states and the bulk-originated QWSs are substantially different that the electrons of two branches are localized on the opposite sides of the crystal in the former system but are spread on one surface in the latter case. By introducing new states (QWSs) between the well-defined surface state (TSS) and the bulk bands, this offers a way to examine the connection between the bulk

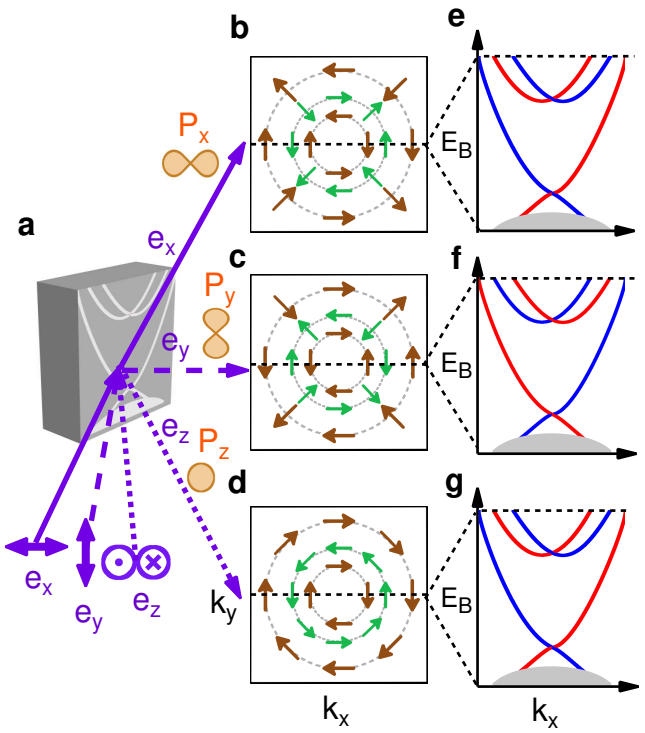

FIG. 3. **(a)** The selected orbitals by linearly polarized light. The solid, dashed, and broken arrows depict that p_i orbital is selected by $\hat{e}_i$, where $i = x, y, z$, respectively. **(b-d)** The p_x, p_y, p_z orbital-entangled spin textures of the QWSs and TSS bands projected on the Fermi surface. **(e-g)** The phenomenological picture of the expected S_y-resolved band dispersion along $k_y = 0$ ($\bar{\Gamma}$-$\bar{M}$) direction.

and the surfaces[31,33], whose close relation can be supported by the great resemblance between QWSs and the topologically trivial gapped surface states.

The mechanism of the spin selection by photon polarization is schematically illustrated in Fig. 3. The photoemission matrix elements, which are dependent on the direction of incident photon vector and the mirror plane where electrons are photoemitted, lead to the optical selection rules[35]. Specifically, linearly polarized photons will only allow $p \rightarrow s$ transitions, and only p_i orbitals will be photoemitted by $\hat{e}_i$ polarized light, where $i = x, y, z$ (demonstrated in Fig. 3(a)). Fig. 3(b-d) show the in plane spin textures that are coupled to the $p_{x,y,z}$-orbitals, respectively. These can be calculated from the eigenstates derived from matrix elements of the effective Hamiltonian. The arrows lying on the three dashed circles depict the projected spins of the inner QWS, outer QWS, and TSS bands on the Fermi surface. Fig. 3(e-g) phenomenologically shows the expected S_y-spin-resolved band dispersion maps along $k_y = 0$ ($\bar{\Gamma}$-$\bar{M}$ direction) from the corresponding orbital-entangled spin textures in (e-g). Notice that the spin orientations between p_x- and p_z-entangled spin textures (Fig. 3(b)(d)) along this cut are identical. This consistency is essential to the observed opposite spin polarization of the whole surface states under our experimental geometry: the p-polarized light will photoemit a mixture of two orbitals yet with the same spin characteristics along $k_y = 0$, whereas the s-polarized photons will photoemit orbitals that carry the opposite spins.

Here we want to emphasize that the observed spin inversion with respect to the rotation of linear photon vector is a pure result of the symmetries and carrier orbitals instead of the topological properties of Bi_2Se_3[21]. This can be supported by the spin-orbital entanglement of Bi_2Se_3 in its topologically trivial phase[33,34]. In fact, similar observations have been reported from other systems with strong intrinsic Rashba-type SOI including conventional[26] and bulk[25] Rashba systems, surface alloy Bi/Ag(111)[27], and topological materials[28] by applying a similar theoretical framework. Although additional mixing of orbitals may contribute complexities to the calculations[27,28], our results and these studies show that selection of spin by polarized light is possible, in principle, with careful investigation of the crystal symmetries, carrier orbitals, and the choice of measured spin components.

V. CONCLUSIONS

Our photon-polarization-dependent SARPES measurements on Bi_2Se_3 reveal the orbital-resolved spin textures of the whole surface states. Due to the bulk origin of the QWSs, the uniform spin-orbital characteristic of TSS and QWSs not only suggests a single origin of the spin inversion of these bands but also implies a surface-bulk connectivity in Bi_2Se_3 which is in agreement with the observed alternating spin helicities. These results provide new important information on the emergence of the TSS state with the bulk state and are fundamental to better understand the interaction between charge and spin transport for the design of next generation TI based devices. Indeed, the development of QWSs not only means additional Fermi surface sheets but also the onset of back scattering channels that can complicate the spin character and the mobility of the carriers in a device. As Bi_2Se_3 has become a prototypical topological material that plays a key role in heterostructure systems, we hope the present work will provide an important insight to the design of TI/Rashba-based devices and the interpretation of their performance.

ACKNOWLEDGMENTS

We thank Z. Li for meaningful discussions. This work was supported by the U.S. Department of Energy (DOE), Office of Science, Office of Basic Energy Sciences, Materials Sciences and Engineering Division, under Contract No. DE-AC02-05CH11231 within the Quantum Materials Program (KC2202) and by the National Science Foundation Grant No. DMR-1410660.

* chiuyunlin@lbl.gov
† kgotlieb@lbl.gov
‡ cmjozwiak@lbl.gov
§ zhussain@lbl.gov
¶ alanzara@lbl.gov

[1] H. Zhang, C.-X. Liu, X.-L. Qi, X. Dai, Z. Fang, and S.-C. Zhang, Nat Phys **5**, 438 (2009).
[2] J. E. Moore, Nature **464**, 194 (2010).
[3] M. Z. Hasan and C. L. Kane, Rev. Mod. Phys. **82**, 3045 (2010).
[4] S. Datta and B. Das, *Applied Physics Letters*, Appl. Phys. Lett. **56**, 665 (1990).
[5] I. Žutić, J. Fabian, and S. Das Sarma, Rev. Mod. Phys. **76**, 323 (2004).
[6] C. Nayak, S. H. Simon, A. Stern, M. Freedman, and S. Das Sarma, Rev. Mod. Phys. **80**, 1083 (2008).
[7] K. D. Petersson, L. W. McFaul, M. D. Schroer, M. Jung, J. M. Taylor, A. A. Houck, and J. R. Petta, Nature **490**, 380 (2012).
[8] C. Jozwiak, C.-H. Park, K. Gotlieb, C. Hwang, D.-H. Lee, S. G. Louie, J. D. Denlinger, C. R. Rotundu, R. J. Birgeneau, Z. Hussain, and A. Lanzara, Nature Physics **9**, 293 (2013).
[9] R. Yu, W. Zhang, H.-J. Zhang, S.-C. Zhang, X. Dai, and Z. Fang, Science **329**, 61 (2010).
[10] J. G. Checkelsky, R. Yoshimi, A. Tsukazaki, K. S. Takahashi, Y. Kozuka, J. Falson, M. Kawasaki, and Y. Tokura, Nature Physics **10**, 731 (2014).
[11] J. W. McIver, D. Hsieh, H. Steinberg, P. Jarillo-Herrero, and N. Gedik, Nature Nanotechnology **7**, 96 (2011).
[12] W.-K. Tse and A. H. MacDonald, Phys. Rev. Lett. **105**, 057401 (2010).
[13] L. A. Wray, S.-Y. Xu, Y. Xia, D. Hsieh, A. V. Fedorov, Y. S. Hor, R. J. Cava, A. Bansil, H. Lin, and M. Z. Hasan, Nat Phys **7**, 32 (2011).
[14] P. D. C. King, R. C. Hatch, M. Bianchi, R. Ovsyannikov, C. Lupulescu, G. Landolt, B. Slomski, J. H. Dil, D. Guan, J. L. Mi, E. D. L. Rienks, J. Fink, A. Lindblad, S. Svensson, S. Bao, G. Balakrishnan, B. B. Iversen, J. Osterwalder, W. Eberhardt, F. Baumberger, and P. Hofmann, Phys. Rev. Lett. **107**, 096802 (2011).
[15] M. Bianchi, R. C. Hatch, J. Mi, B. B. Iversen, and P. Hofmann, Phys. Rev. Lett. **107**, 086802 (2011).
[16] T. Valla, Z.-H. Pan, D. Gardner, Y. S. Lee, and S. Chu, Phys. Rev. Lett. **108**, 117601 (2012).
[17] H. M. Benia, C. Lin, K. Kern, and C. R. Ast, Phys. Rev. Lett. **107**, 177602 (2011).
[18] M. Bianchi, R. C. Hatch, D. Guan, T. Planke, J. Mi, B. B. Iversen, and P. Hofmann, Semiconductor Science and Technology **27**, 124001 (2012).
[19] C. Jozwiak, J. Graf, G. Lebedev, N. Andresen, A. K. Schmid, A. V. Fedorov, F. El Gabaly, W. Wan, A. Lanzara, and Z. Hussain, Review of Scientific Instruments **81**, 053904 (2010), http://dx.doi.org/10.1063/1.3427223.
[20] K. Gotlieb, Z. Hussain, A. Bostwick, A. Lanzara, and C. Jozwiak, Review of Scientific Instruments **84**, 093904 (2013), http://dx.doi.org/
[21] C.-H. Park and S. G. Louie, Phys. Rev. Lett. **109**, 097601 (2012).
[22] H. Zhang, C.-X. Liu, and S.-C. Zhang, Phys. Rev. Lett. **111**, 066801 (2013).
[23] A. Damascelli, Z. Hussain, and Z.-X. Shen, Rev. Mod. Phys. **75**, 473 (2003).
[24] Y. Cao, J. A. Waugh, X.-W. Zhang, J.-W. Luo, Q. Wang, T. J. Reber, S. K. Mo, Z. Xu, A. Yang, J. Schneeloch, G. D. Gu, M. Brahlek, N. Bansal, S. Oh, A. Zunger, and D. S. Dessau, Nat Phys **9**, 499 (2013).
[25] H. Maasz, H. Bentmann, C. Seibel, C. Tusche, S. V. Eremeev, T. R. F. Peixoto, O. E. Tereshchenko, K. A. Kokh, E. V. Chulkov, J. Kirschner, and F. Reinert, Nat Commun **7**, (2016).
[26] K. Miyamoto, H. Wortelen, H. Mirhosseini, T. Okuda, A. Kimura, H. Iwasawa, K. Shimada, J. Henk, and M. Donath, Phys. Rev. B **93**, 161403 (2016).
[27] S. N. P. Wissing, A. B. Schmidt, H. Mirhosseini, J. Henk, C. R. Ast, and M. Donath, Phys. Rev. Lett. **113**, 116402 (2014).
[28] K. Gotlieb, Z. Li, C.-Y. Lin, C. Jozwiak, J. H. Ryoo, C.-H. Park, Z. Hussain, S. G. Louie, and A. Lanzara, Phys. Rev. B **95**, 245142 (2017).
[29] S. LaShell, B. A. McDougall, and E. Jensen, Phys. Rev. Lett. **77**, 3419 (1996).
[30] C. Jozwiak, Y. L. Chen, A. V. Fedorov, J. G. Analytis, C. R. Rotundu, A. K. Schmid, J. D. Denlinger, Y.-D. Chuang, D.-H. Lee, I. R. Fisher, R. J. Birgeneau, Z.-X. Shen, Z. Hussain, and A. Lanzara, Phys. Rev. B **84**, 165113 (2011).
[31] M. Bahramy, P. King, A. de la Torre, J. Chang, M. Shi, L. Patthey, G. Balakrishnan, P. Hofmann, R. Arita, N. Nagaosa, and F. Baumberger, Nat Commun **3**, 1159 (2012).
[32] C. Jozwiak, J. A. Sobota, K. Gotlieb, A. F. Kemper, C. R. Rotundu, R. J. Birgeneau, Z. Hussain, D.-H. Lee, Z.-X. Shen, and A. Lanzara, **7**, 13143 (2016).
[33] S.-Y. Xu, M. Neupane, I. Belopolski, C. Liu, N. Alidoust, G. Bian, S. Jia, G. Landolt, B. Slomski, J. H. Dil, P. P. Shibayev, S. Basak, T.-R. Chang, H.-T. Jeng, R. J. Cava, H. Lin, A. Bansil, and M. Z. Hasan, **6**, 6870 (2015).
[34] G. Landolt, S. Schreyeck, S. V. Eremeev, B. Slomski, S. Muff, J. Osterwalder, E. V. Chulkov, C. Gould, G. Karczewski, K. Brunner, H. Buhmann, L. W. Molenkamp, and J. H. Dil, Phys. Rev. Lett. **112**, 057601 (2014).
[35] A. M. Turner, A. W. Donoho, and J. L. Erskine, Phys. Rev. B **29**, 2986 (1984).